ARTICLES
https://doi.org/10.1038/s41561-017-0010-7
nature geoscience

Fossil intermediate-depth earthquakes in subducting slabs linked to differential stress release

Marco Scambelluri[1*], Giorgio Pennacchioni[2], Mattia Gilio[1,3], Michel Bestmann[4], Oliver Plümper[5] and Fabrizio Nestola[2]

The cause of intermediate-depth (50–300 km) seismicity in subduction zones is uncertain. It is typically attributed either to rock embrittlement associated with fluid pressurization, or to thermal runaway instabilities. Here we document glassy pseudotachylyte fault rocks—the products of frictional melting during coseismic faulting—in the Lanzo Massif ophiolite in the Italian Western Alps. These pseudotachylytes formed at subduction-zone depths of 60–70 km in poorly hydrated to dry oceanic gabbro and mantle peridotite. This rock suite is a fossil analogue to an oceanic lithospheric mantle that undergoes present-day subduction. The pseudotachylytes locally preserve high-pressure minerals that indicate an intermediate-depth seismic environment. These pseudotachylytes are important because they are hosted in a near-anhydrous lithosphere free of coeval ductile deformation, which excludes an origin by dehydration embrittlement or thermal runaway processes. Instead, our observations indicate that seismicity in cold subducting slabs can be explained by the release of differential stresses accumulated in strong dry metastable rocks.

Over a total length of ~55,000 km, subduction zones at convergent plate margins are the main setting for earthquakes globally. In such environments, seismicity is caused by accumulation and release of stress from shallow levels down to intermediate depths (50–300 km) (refs [1–3]). Intermediate-depth earthquakes are inaccessible to direct investigation and much knowledge relies on seismic data, rock-deformation experiments and modelling. Geophysical data show that the seismic activity in subduction zones concentrates either inside the subducting lithosphere, or in thick (kilometres) layers along the plate interface. These layers consist of hydrated rocks that host pressurized pore fluids and show low seismic velocities[4–7]. Experimental work and numerical models suggest that subduction-zone seismicity is triggered by a thermal runaway instability[8–12], dehydration embrittlement[2,13,14], phase transformation[15] or the reactivation of earlier discontinuities[1]. To date, investigations have focused prevalently on seismicity in the subducting oceanic crust and in the low-velocity plate interface[2,4,5,13–15], whereas the seismic potential of the lithospheric mantle of subducting oceanic plates remains poorly understood.

Compared with the above studies, field-based investigations of exhumed high-pressure rocks have so far been underutilized to study fossilized earthquake phenomena directly. Pseudotachylytes, the solidified friction-induced melts produced during seismic slip along a fault, are unique indicators of palaeo-earthquakes in exhumed faults. Unfortunately, pseudotachylytes are rarely preserved in the rock record and the examples related to subduction settings are limited to findings within exhumed blueschist- and eclogite-facies continental and oceanic crust sections[16–22].

Here we investigate pseudotachylytes in a gabbro–peridotite body from the Lanzo Massif (Italian Western Alps), a tectonic slice of oceanic mantle involved in Alpine subduction. These pseudotachylytes were previously attributed to a pre-subduction oceanic detachment setting[23,24], but here we conclude they formed under eclogite-facies conditions. Although similar to pseudotachylytes from Corsica, related to blueschist-facies metamorphism at shallower subduction depths[19–22,25], our case study provides a unique record of oceanic slab eclogitization in the Wadati–Benioff seismic zone, in analogy with the intermediate-depth seismicity that affects the lithospheric mantle in present-day subducting slabs.

The host rocks of fossil seismic faults

The Alpine Lanzo Massif is a 20×9 km sliver of oceanic mantle peridotite with subordinated 160 Ma old gabbro dykes[23], regionally embedded in serpentinite and metagabbro (Supplementary Fig. 1). It records oceanic serpentinization around unaltered peridotite cores[26] and later subduction-related Alpine metamorphism under eclogite-facies conditions (2–2.5 GPa and 550–620 °C at 55–46 Ma) (refs [26–29]). The southernmost body of the Lanzo Massif (Moncuni (Supplementary Fig. 1)) has a core of poorly hydrated to anhydrous mantle peridotite and pyroxenite intruded by dykes (centimetres to tens of centimetres thick) of preserved dry gabbro. Such unaltered gabbro and peridotite are predominant in Moncuni, and contain minor volumes (~5 vol%) of hydrated metaperidotite and metagabbro that record static eclogite-facies metamorphism. The heterogeneous water distribution can be related to limited oceanic hydration prior to subduction. Unaltered and hydrated eclogitized domains form a coherent body that underwent the same subduction-zone evolution, but the predominant peridotite and gabbro metastably escaped eclogitization. Hence, most oceanic lithosphere in Moncuni, as in the whole Lanzo Massif, metastably preserved the

[1]Dipartimento di Scienze della Terra, Ambiente e Vita, University of Genova, Genoa, Italy. [2]Dipartimento di Geoscienze, University of Padova, Padua, Italy. [3]Dipartimento di Scienze della Terra e dell'Ambiente, University of Pavia, Pavia, Italy. [4]GeoZentrum Nordbayern, Friedrich-Alexander University of Erlangen-Nürnberg, Erlangen, Germany. [5]Department of Earth Sciences, Utrecht University, Utrecht, The Netherlands.
*e-mail: marco.scambelluri@dipteris.unige.it

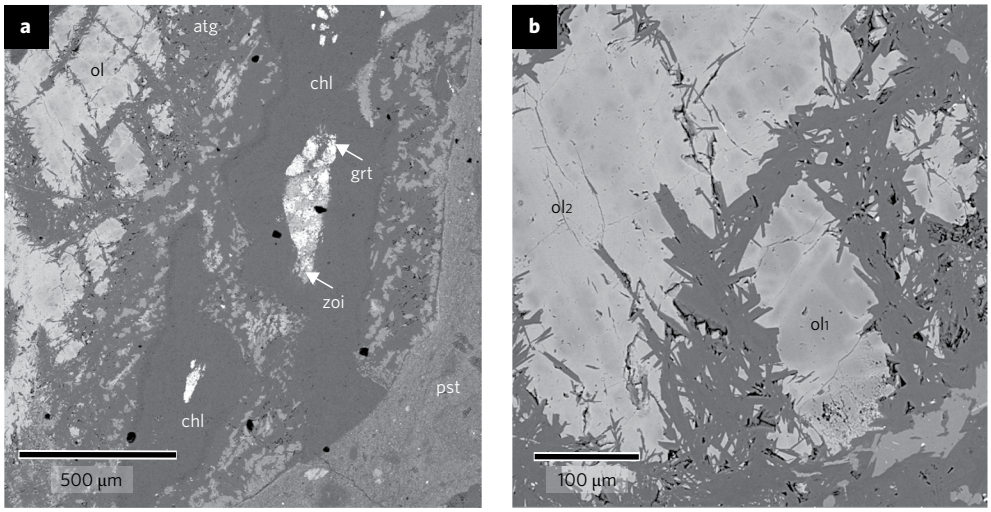

Fig. 1 | Pseudotachylyte in eclogitized metaperidotite. a, SEM back-scattered image of pseudotachylyte (pst) cutting across olivine (ol), which is partially replaced by antigorite (atg). Mantle plagioclase has been replaced by metamorphic garnet (grt), zoisite (zoi) and chlorite (chl). **b**, Close-up of the olivine shown in **a** reveals darker relict cores of mantle olivine (ol1; Mg no. = 0.89–0.91) replaced by lighter metamorphic olivine along the rim and microfractures (ol2; Mg no. = 0.82–0.86).

pristine structures and mineral assemblages representative of pre-subduction mantle and oceanic settings throughout its 100 Myr-long history. Very limited water access during the entire evolution thus prevented the metamorphic re-equilibration of poorly hydrated to anhydrous rock domains and the ductile deformation of the entire rock mass during subduction.

The unaltered peridotite comprises olivine, orthopyroxene, clinopyroxene and spinel that show a coarse pre-oceanic mantle tectonite foliation[23]. This rock is enriched in plagioclase because of the melt–rock reaction during the mantle-to-ocean evolution[23] and, in addition, can display minor amounts of amphibole[23] and serpentine. The unaltered gabbro dykes display igneous clinopyroxene, olivine and plagioclase, locally overprinted by an oceanic high-temperature (700–800 °C) mylonitic foliation[24] (Supplementary Fig. 2). The high-temperature, pre-subduction mantle-to-oceanic foliations are the only ductile deformation structures developed in these rocks.

In the Moncuni eclogitic metaperidotite, mantle olivine and plagioclase were statically replaced by metamorphic olivine + antigorite and by zoisite + garnet + chloritoid + chlorite, respectively (Fig. 1a,b). In the eclogitic metagabbros, igneous plagioclase was pseudomorphosed by jadeite + zoisite + garnet + kyanite, olivine by talc + tremolite and clinopyroxene by omphacite; chloritoid coronas formed between pseudomorphosed plagioclase and olivine. Such transformations are typical of Alpine eclogitic metagabbros and metaperidotites[26–30].

Relative timing and *P–T* earthquake faulting conditions

Numerous pseudotachylyte veins cross-cut the Moncuni peridotite, pyroxenite and gabbro, the derived high-temperature tectonite and mylonite, and the eclogitic metaperidotite and metagabbro. Pseudotachylytes occur as moderately to steeply dipping fault veins, striking N–S to NW–SE, trending subparallel to the main set of gabbro but also locally cross-cutting the dykes. The pseudotachylyte fault veins are associated with subparallel, pervasive, sharp and brittle slip planes and thin cataclasites, all cross-cutting the pre-existing tectonitic (peridotite), magmatic and mylonitic (gabbro) fabrics. Pseudotachylytes in rocks that host even trace amounts of water (poorly hydrated peridotite, eclogitic metaperidotite and metagabbro) do not contain glass, but a crypto- to microcrystalline matrix. Glass is only preserved in pseudotachylytes within dry, unaltered gabbros. The thickest pseudotachylyte veins (a few tens of centimetres (Fig. 2a)) occur in peridotite: the matrix and microlites entirely annealed to an aggregate of olivine, orthopyroxene, clinopyroxene and Cr-spinel (Fig. 2b). This agrees with previous description of orthopyroxene, olivine, interstitial clinopyroxene and spinel microlites in such pseudotachylytes[23,24], and suggests cooling and post-cooling recrystallization of the frictional melt in the spinel stability field for ultramafic systems.

In gabbros, mylonitic gabbros (Supplementary Fig. 2), and eclogitic metagabbros (Fig. 2c), the pseudotachylyte fault and injection veins are a few micrometres to a few millimetres thick. In gabbros and gabbro mylonites, the rock-forming minerals display a pervasive shattered microstructure and brittle comminution close to microfaults and pseudotachylytes, and occur as unreacted clasts within cataclasites (Supplementary Figs. 3 and 4) and pseudotachylytes. Pseudotachylyte fault and injection veins cut the cataclastic zones and truncate all the minerals (Supplementary Figs. 5 and 6). Other than a cataclastic flow structure, the wall-rock minerals aside the faults and pseudotachylytes do not show evidence of progressive grain-size reduction by dynamic recrystallization (Supplementary Figs. 5 and 6). In pristine gabbros, pseudotachylytes consist of glass that includes microlites of clinopyroxene, plagioclase, garnet and fragments of the host rock that lack kinking and foliation planes. Figure 3a shows two glassy pseudotachylyte fault veins with protruding injection veins cutting a gabbro. The larger vein shows a flow layering with a band of pure glass (white dotted line, Fig. 3a) and a band of clast-laden glass clustered with plagioclase and clinopyroxene microlites (a few micrometres in size). Microlites also occur in trails along healed microcracks confined within the pseudotachylyte. Raman analysis shows the pseudotachylyte glass is anhydrous (Supplementary Fig. 7). Micrometric pyrope-rich garnet associates with plagioclase and clinopyroxene microlites (Fig. 3b–d and Supplementary Fig. 8). Garnet also occurs in rare discontinuous coronas, a few micrometres wide, at plagioclase–olivine boundaries only in the gabbro wall rocks adjacent to the pseudotachylyte veins (Fig. 3a). This corona–garnet acted as a nucleation site for garnet microlites that overgrew the pseudotachylyte glass (Fig. 3e). Pseudotachylyte in pyroxenite contains pyrope-rich garnet microlites with a dendritic shape, which suggests growth from quenched frictional melts[31,32] (Fig. 3f and Supplementary Fig. 9). In unaltered gabbro, garnet is thus restricted to pseudotachylytes and grew either inside the veins or in the adjacent wall rock. The

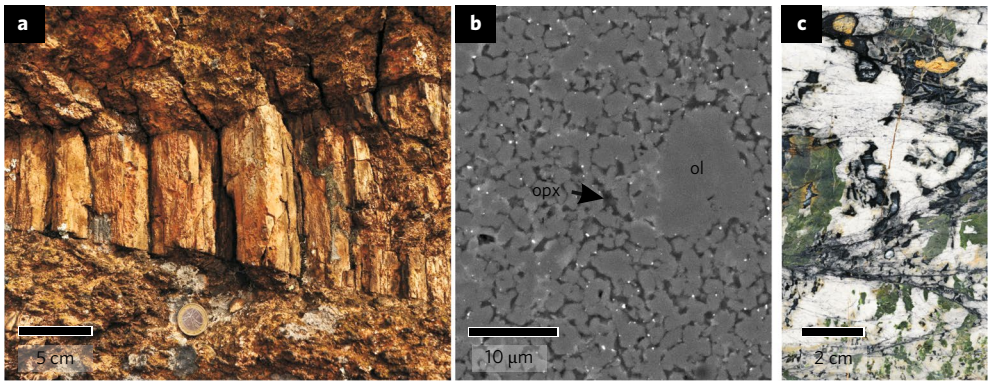

Fig. 2 | Pseudotachylyte in peridotite and metagabbro. a, Pseudotachylyte vein within peridotite. **b**, SEM back-scattered image showing small microlites of olivine (ol), orthopyroxene (opx, dark grey), clinopyroxene (light grey) and spinel (small bright droplets). A large olivine clast is included in the groundmass. **c**, Photograph of a polished sample showing black millimetre-thick pseudotachylyte veins cutting the eclogitic metagabbro. The igneous clinopyroxene, plagioclase and olivine in the metagabbro have been pseudomorphosed by green omphacite, white jadeite + zoisite and black chlorite + chloritoid with cores of white talc, respectively (Supplementary Section 1).

major element compositions of such garnets are all comparable with those of eclogitic garnet from other Alpine gabbros with similar bulk composition (Supplementary Fig. 10). This helps to bracket pseudotachylyte formation within a stage of high-pressure garnet growth.

The eclogitic metagabbro and metaperidotite domains at Moncuni are limited in volume, but their relationships with pseudotachylyte are fundamental to assess the tectonic environment of seismic faulting. Figure 4a shows pseudotachylyte veins and sub-parallel microfaults that dissect the contact between metagabbro and metaperidotite. Within the metagabbro, these microfaults offset cataclastic igneous pyroxene cemented by omphacite (Fig. 4b) and cut the jadeite + zoisite pseudomorphs after plagioclase (Fig. 4a). The microfaults contain clastic fragments of jadeite and zoisite replacing plagioclase and are overgrown by eclogite-facies dendritic garnet (Supplementary Figs. 12–14, and garnet composition given in Supplementary Fig. 10). Garnet growth near the pseudotachylytes and microfaults was probably enhanced by the thermal transient caused by frictional heating.

In metaperidotite, the pseudotachylyte matrix consists of olivine and pyroxene microlites variably altered into serpentine, talc and tremolite. These pseudotachylytes cut prograde antigorite veins (Supplementary Fig. 15) and include: (1) clasts of mantle olivine overgrown by high-pressure metamorphic olivine (Fig. 4c, (2)) olivine clasts that host antigorite veinlets truncated against the pseudotachylyte (Fig. 4d) and (3) high-pressure pseudomorphs after the mantle plagioclase corroded by the pseudotachylyte melt (Fig. 4d and Supplementary Fig. 16). Olivine microlites display higher Mg concentrations than the host-rock olivine (Supplementary Fig. 17). Late-stage veins that cut the metagabbro, metaperidotite and pseudotachylyte

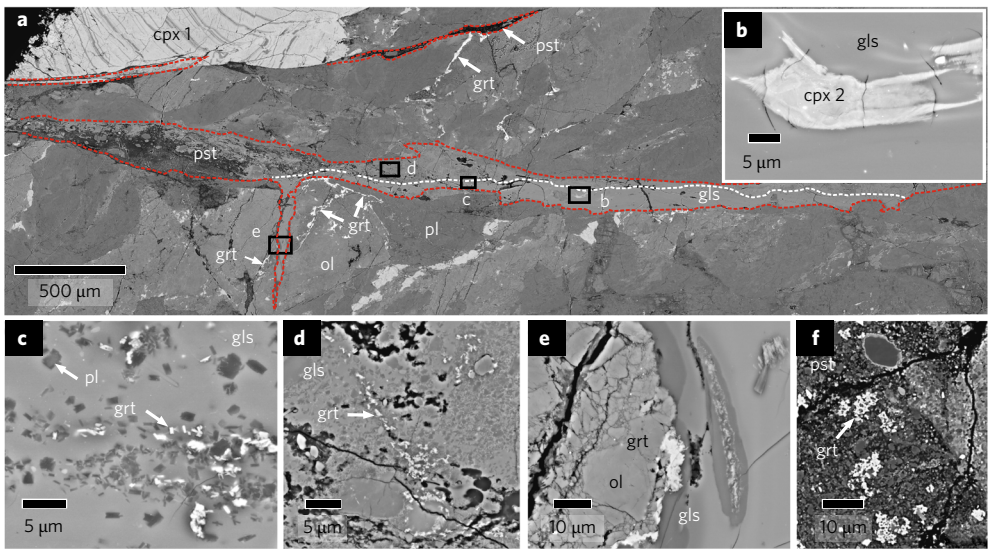

Fig. 3 | Pseudotachylyte in anhydrous gabbro. Back-scattered SEM images of Supplementary Fig. 6. **a**, Pseudotachylyte fault vein (outlined by red dashed lines) that cuts a gabbro preserving magmatic clinopyroxene (cpx1), olivine (ol) and plagioclase (pl). Metamorphic garnet (grt) coronas formed at olivine–plagioclase boundaries close to pseudotachylyte (white arrows). The fault and associated injection vein contain pure glass layers (under the white dashed line) and near-glass layers that included microlites and clasts. **b**,**c**, Pseudotachylyte glass (gls) hosting dendrite-like clinopyroxene microlites (cpx2) (**b**) with plagioclase and garnet microlites (**c**). **d**, Garnet microcracks in glassy pseudotachylyte. **e**, Host-rock garnet overgrowing the glassy pseudotachylyte. **f**, Dendrite-like garnet in pseudotachylyte from pyroxenite.

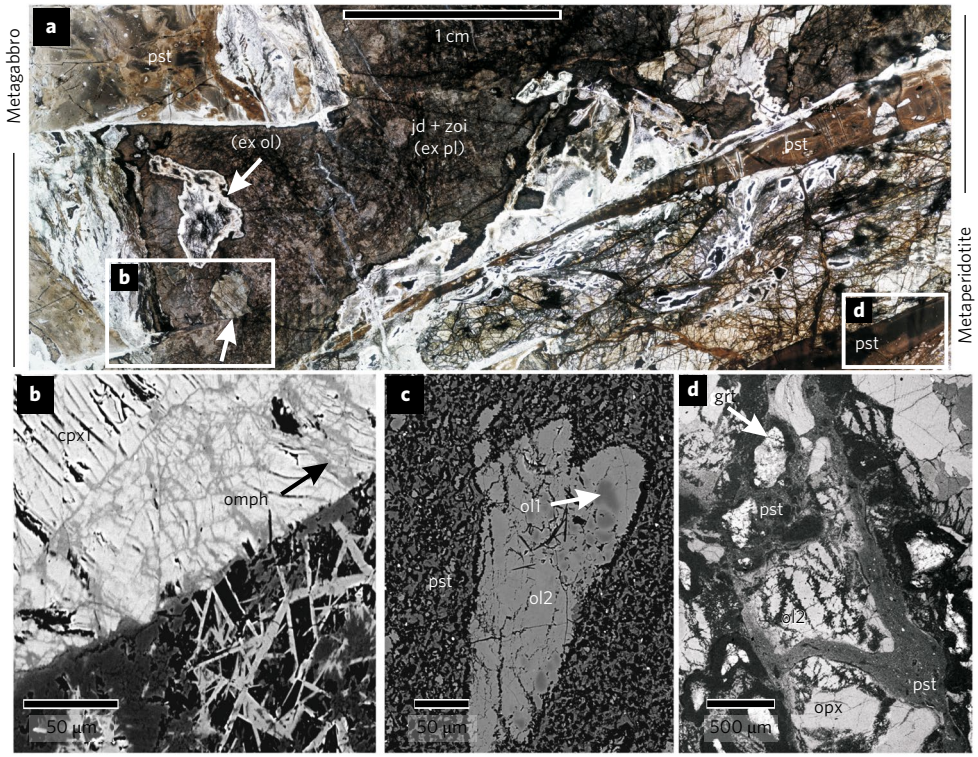

Fig. 4 | Pseudotachylyte in metaperidotite–metagabbro. a, Transmitted light image of pseudotachylyte (pst) at metaperidotite–metagabbro contact. In the metagabbro, jadeite + zoisite (jd + zoi) replaced plagioclase, talc + chloritoid replaced olivine (ex ol) and omphacite replaced clinopyroxene (detail in **b**). In the metaperidotite, metamorphic olivine (ol2) and antigorite replaced mantle olivine (ol1) and garnet + zoisite + chlorite replaced plagioclase. The white arrow (**b**) indicates a microfault parallel to pseudotachylyte. **b**, Enlargement of rectangle **b** in **a**. The microfault offsets cataclastic igneous clinopyroxene (cpx1) cemented by omphacite (omph). **c**, SEM back-scattered image of pseudotachylyte hosting clasts of mantle ol1 overgrown by ol2. **d**, Enlargement of rectangle **d** in **a**. Pseudotachylyte enclosing clasts of ol2 + antigorite + orthopyroxene (opx) and disrupted fragments of garnet-bearing pseudomorphs after plagioclase (Supplementary Fig. 8).

(Fig. 4a) display high-pressure mineralogy: the same vein contains zoisite + chlorite + omphacite in the metagabbro and talc + tremolite in the ultramafic pseudotachylyte (Supplementary Fig. 18a–c). Pseudotachylyte and microfaults thus cut eclogitized metagabbro and metaperidotite (Fig. 4), and are in turn overgrown by eclogitic garnet and cut by high-pressure veins (Supplementary Figs. 12 and 18).

Pressure–temperature estimates for Lanzo eclogitic metagabbros[28] yield 2–2.5 GPa and 550–620 °C, which corresponds to a 8 °C km^{-1} gradient similar to that of modern subduction zones[33]. In metaperidotite, the formation of secondary olivine via the reaction antigorite + brucite = olivine + fluid[26,30] and the breakdown of mantle plagioclase into chlorite, zoisite and garnet occurred at comparable conditions of 2–2.5 GPa and 600 °C (ref. [26]). Pressure–temperature estimates made for the Moncuni hydrated eclogitized metagabbro and metaperidotite yield similar values. We calculated the mineral phase stabilities using the hydrated eclogitized rock compositions, because they represent the only water-saturated reactive volumes that equilibrated under the eclogite-facies conditions. A maximum of 2.2 GPa and 600 °C are achieved for the crystallization of omphacite, zoisite, garnet and kyanite after the gabbro plagioclase (Supplementary Fig. 18d). The formation of talc + tremolite in veins that cut the ultramafic pseudotachylyte occurred below 2.2 GPa (Supplementary Fig. 18e).

In the gabbros, the pyrope content of the garnet microlites and eclogitic garnet growth after the pseudotachylyte glass (Fig. 3e) suggest that faulting occurred in the stability field of the eclogitic garnet. In eclogitized rocks, the omphacite-cemented breccia (Fig. 4b), entrainment of eclogitic mineral clasts in pseudotachylyte and microfaults (Fig. 4c,d), eclogitic garnet overgrowth of microfaults in metagabbro (Supplementary Figs. 12–14) and high-pressure veins that cut the pseudotachylytes (Supplementary Fig. 18d,e) all suggest eclogite-facies intermediate-depth seismic faulting at ~70 km depth.

Potential mechanism for intermediate depth seismicity

The Moncuni pseudotachylyte occurs in ophiolitic gabbro–peridotite that records the pre-subduction high-temperature ductile deformation during mantle flow and oceanic mylonitization[23,24]. We did not observe any crystal–plastic flow referable to subduction (Supplementary Fig. 6). All the studied rocks display either mantle tectonite fabrics or gabbroic igneous and mylonitic oceanic textures. The entire Alpine subduction zone recrystallization took place statically and produced pseudomorphic and coronitic textures (Figs. 1a, 2c, 4a and Supplementary Fig. 11). All the rocks escaped ductile deformation (and local metamorphism) during the subduction when the coseismic rupture and frictional melting took place. The mechanical response, the metastable survival of pre-subduction mineral assemblages and the preservation of dry pseudotachylyte glass imply that this rock package experienced very limited hydration. Our observations highlight the intimate link between seismic activity and strong, poorly hydrated metastable sections of the subducted oceanic lithosphere. This allows us to constrain the seismogenic environment and discuss the mechanism that triggered the intermediate-depth seismicity recorded at Moncuni.

Thermal runaway and dehydration embrittlement are the earthquake mechanisms most accredited by geoscientists. Present-day intermediate-depth earthquakes in the mantle have been related to thermal runaway[34,35]. This mechanism explains the synkinematic

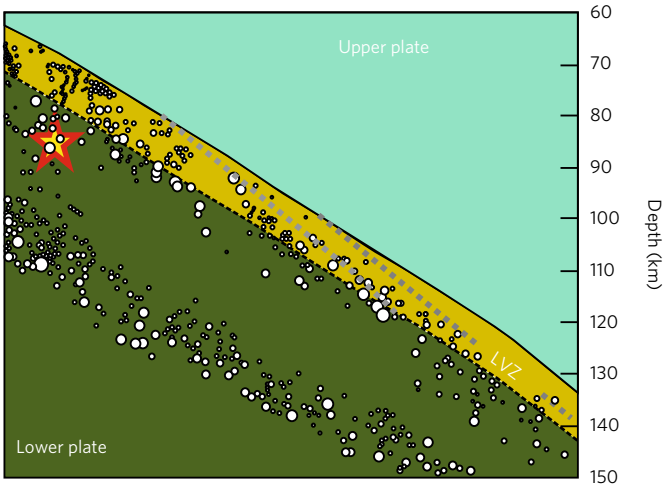

Fig. 5 | Locating the seismic activity of Moncuni in a subducting slab. Seismicity in a subduction zone (modified from Kita et al.[42]). The brown layer corresponds to the low-velocity zone (LVZ); the light green and dark green fields represent the mantle wedge and the subducting oceanic mantle, respectively. The light grey dashed lines in the LVZ correspond to dehydration boundaries that separate the amphibole–lawsonite eclogite (shallow LVZ, left side) from the jadeite–lawsonite eclogite (central LVZ) and the jadeite–lawsonite eclogite from the anhydrous eclogite (deeper part of LVZ, right side). Circles show hypocentres in the LVZ and in the subducting plate. The star shows the interpreted location of the Moncuni seismic failure.

association of pseudotachylyte and mylonites: in blueschist-facies gabbro–peridotite from Corsica, the pseudotachylyte was synchronous with mylonitization of the wall rocks. This is indicated (1) by the foliation development and grain-size reduction via dynamic recrystallization in rock domains near fault planes, and (2) by the entrainment of deformed wall-rock fragments in pseudotachylyte veins[21,22]. Such evidence enabled the faulting to be linked to localized crystal–plastic deformation and thermal runaway under stress of up to 580 MPa or more[21,22,36]. Moncuni pseudotachylytes invariably cut pre-subduction foliated peridotite and gabbro, as well as undeformed massive rocks. The absence of an eclogite-facies mylonitic foliation and of dynamic recrystallization in the selvages of the fault veins, and the lack of foliated eclogitized rock fragments inside pseudotachylytes suggest that Moncuni, different from Corsica, does not record a crystal–plastic deformation precursory to seismic slip. The dry-glass composition, moreover, indicates that little water was available to promote ductile shearing[11]. Overall, the above features suggest that the frictional melting at Moncuni was not caused by a thermal runaway shear instability.

Regarding dehydration-induced seismic embrittlement, laboratory experiments that investigated the behaviour of dehydrating serpentinite by monitoring acoustic signals provide contrasting results. Whereas some experiments report that serpentine dehydration produces acoustic emissions[13,37], others show that dehydration occurs without embrittlement and acoustic activity[38,39]. Recent deformation experiments on dehydrating synthetic aggregates of antigorite + olivine show that acoustic emissions associated with shear failure can occur in samples that contain small amounts of antigorite (5 vol%) (ref. [40]). These results show that little dehydration is necessary to trigger seismicity and suggest that dehydration-induced stress transfer, rather than fluid overpressure, causes embrittlement[40]. Comparably, Moncuni hosts ~5 vol% hydrated metaperidotite that records the initial antigorite dehydration to secondary olivine (Fig. 1a), which produced only 2 wt% fluid from fully serpentinized rocks[30]. The amount of water released by the volumetrically subordinate metaperidotite is thus insufficient to induce extensive seismic faulting in the whole Moncuni body. The presence of metamorphic olivine clasts within the pseudotachylyte (Fig. 4c) may even suggest that antigorite dehydration pre-dated the seismic activity. The Moncuni eclogitic metagabbro does not contain amphibole and/or lawsonite (whose dehydration is suggested to cause seismic embrittlement in the crustal section of subducting slabs[14]), and the cross-cutting cataclasite and microfaults entrain zoisite clasts that are stable during the eclogite-facies event (Supplementary Figs. 12 and 13). Consequently, rock embrittlement caused by fluid overpressure does not represent a viable mechanism to explain the seismicity at Moncuni. Instead, as achieved in deformation experiments[40], shear failure may have occurred in strong peridotite (and gabbro) that hosted minor dehydrating antigorite domains. As suggested by the experimental modelling[40], dehydrating antigorite domains lost their load capacity and transferred stress to the surrounding peridotite, which induced instability and faulting in the olivine-rich rock asperities[40]. Stress propagation out of the minor dehydrating metaperidotite volumes, or from the serpentinite enclosing the Moncuni body, into unaltered peridotite and gabbro may thus explain the formation of the observed pseudotachylytes.

Moreover, the pressure–temperature conditions of the Moncuni pseudotachylyte formation (Supplementary Fig. 18d,e) coincide with the depth of plate unbending[41]. This process could also have contributed to the enhanced differential stress in the uppermost part of the strong dry slab, which might have exceeded the stress needed for peridotite failure (580 MPa (ref. [36]).

Locating the seismic hypocentre

The distribution of intermediate-depth seismicity in subduction zones shows that seismic events nucleate in low-velocity zones at the plate interface[4,42–45] and inside the subducting plate in the upper Wadati–Benioff zone[4,5,42–45]. The low-velocity zones can consist of (1) altered crustal sections of the slab[5], (2) mélanges of rocks derived from both the subducting slab and overriding plate[5] and (3) large serpentinite slices detached from the slab[46]. Seismic wave velocities in these domains are hampered by the presence of abundant hydrous minerals and pressurized fluids[6,7], which make them preferential sites for seismic dehydration embrittlement[2,13,14] and non-volcanic tremors[47]. In contrast, the Wadati–Benioff seismic zone can be located inside the lower oceanic crust or in the upper lithospheric mantle of subducting plates[5]. In this deeper seismic level, heterogeneous hydration of the mantle rocks can be localized along earlier oceanic detachment faults and/or extensional faults developed during slab bending in the outer rise of subduction zones[48].

Figure 5 helps identify the seismic subduction-zone environment for the Moncuni pseudotachylytes. Moncuni, like the entire Lanzo Massif, differs from the other Alpine ophiolitic complexes, which pervasively equilibrated to high-pressure metamorphic assemblages during subduction[49]. These complexes either derived from the altered upper part of oceanic slabs or from plate interface domains, where extensive metamorphic re-equilibration occurred in the presence of abundant fluids. Pseudotachylytes had not been observed hitherto in serpentinite and other hydrated eclogite-facies rocks, whose potential seismic record is represented by eclogitic breccias[50] related to high fluid pressures. In contrast, the dry and metastable Moncuni and Lanzo peridotite fits a location in the intraslab lithosphere (Fig. 5a), whose structures and behaviour correspond to the available descriptions of eclogitic pseudotachylyte in metastable dry rocks[16,17,31,32]. We thus conclude that strong dry-to-poorly hydrated peridotite and gabbro within subducting slabs can either undergo stress transfer from nearby dehydrating rock domains[40] or accumulate large differential stress during plate unbending[41], which may represent alternative mechanisms to generate intermediate-depth seismicity in subduction-zone environments.

Methods

Methods, including statements of data availability and any associated accession codes and references, are available at https://doi.org/10.1038/s41561-017-0010-7.

Received: 18 July 2017; Accepted: 20 October 2017;
Published online: 27 November 2017

References

1. Kirby, S. H., Engdahl, E. R. & Denlinger R. in *Subduction: Top to Bottom* (eds G. E. Bebout et al.) 195–214 (Geophysics Monograph Series 96, AGU, Washington DC, 1996).
2. Hacker, B. R., Peacock, S. M., Abers, G. A. & Holloway, S. D. Subduction factory 2. Are intermediate-depth earthquakes in subducting slabs linked to metamorphic dehydration reactions? *J. Geophys. Res.* **108**, 2030 (2003).
3. Frohlich, C. The nature of deep-focus earthquakes. *Ann. Rev. Earth Planet. Sci.* **17**, 227–254 (1989).
4. Abers, G. A. Seismic low-velocity layer at the top of subducting slabs: observations, predictions, and systematics. *Phys. Earth Planet. Int.* **149**, 7–29 (2005).
5. Bostock, M. G. The Moho in subduction zones. *Tectonophysics* **609**, 547–557 (2013).
6. Audet, P., Bostock, M. G., Christensen, N. I. & Peacock, S. M. Seismic evidence for overpressured subducted oceanic crust and megathrust fault sealing. *Nature* **457**, 76–78 (2009).
7. Kodaira, S. et al. High pore fluid pressure may cause silent slip in the Nankai Trough. *Science* **304**, 1295–1298 (2004).
8. Ogawa, M. Shear instability in a viscoelastic material as the cause of deep focus earthquakes. *J. Geophys. Res.* **92**, 13801–13810 (1987).
9. Braeck, S. & Podladchikov, Y. Y. Spontaneous thermal runaway as an ultimate failure mechanism of materials. *Phys. Rev. Lett.* **98**, 095504 (2007).
10. Kelemen, P. B. & Hirth, G. A. Periodic shear-heating mechanism for intermediate-depth earthquakes in the mantle. *Nature* **446**, 787–790 (2007).
11. John, T. et al. Generation of intermediate-depth earthquakes by self-localizing thermal runaway. *Nat. Geosci.* **2**, 137–140 (2009).
12. Thielmann, M., Rozel, A., Kaus, B. J. P. & Ricard, Y. Intermediate-depth earthquake generation and shear zone formation caused by grain size reduction and shear heating. *Geology* **43**, 791–794 (2015).
13. Jung, H., Green, H. W. II & Dobrzhinetskaya, L. F. Intermediate-depth earthquake faulting by dehydration embrittlement with negative volume change. *Nature* **428**, 545–549 (2004).
14. Okazaki, K. & Hirth, G. Dehydration of lawsonite could directly trigger earthquakes in subducting oceanic crust. *Nature* **530**, 81–85 (2016).
15. Green, H. W. II, Shi, F., Bozhilov, K., Xia, G. & Reches, Z. Phase transformation and nanometric flow cause extreme weakening during fault slip. *Nat. Geosci.* **8**, 484–490 (2015).
16. Austrheim, H. & Boundy, T. M. Pseudotachylytes generated during seismic faulting and eclogitization of the deep crust. *Science* **265**, 82–83 (1994).
17. Austrheim, H. et al. Fragmentation of wall rock garnets during deep crustal earthquakes. *Sci. Adv.* **3**, e1602067 (2017).
18. John, T. & Schenk, V. Interrelations between intermediate-depth earthquakes and fluid flow within subducting oceanic plates: constraints from eclogite facies pseudotachylytes. *Geology* **34**, 557–560 (2006).
19. Austrheim, H. & Andersen, T. B. Pseudotachylytes from Corsica: fossil earthquakes from a subduction complex. *Terra Nova* **16**, 193–197 (2004).
20. Andersen, T. B. & Austrheim, H. Fossil earthquakes recorded by pseudotachylytes in mantle peridotite from the Alpine subduction complex of Corsica. *Earth Planet. Sci. Lett.* **242**, 58–72 (2006).
21. Deseta, N., Andersen, T. B. & Ashwal, L. D. A weakening mechanism for intermediate-depth seismicity? Detailed petrographic and microtextural observations from blueschist facies pseudotachylytes, Cape Corse, Corsica. *Tectonophysics* **610**, 138–149 (2014).
22. Deseta, N., Ashwal, L. D. & Andersen, T. B. Initiating intermediate-depth earthquakes: insights from a HP–LT ophiolite from Corsica. *Lithos* **206–207**, 127–146 (2014).
23. Piccardo, G. B., Ranalli, G. & Guarnieri, L. Seismogenic shear zones in the lithospheric mantle: ultramafic pseudotachylytes in the Lanzo peridotite (Western Alps, NW Italy). *J. Petrol.* **51**, 81–100 (2010).
24. Piccardo, G. B., Ranalli, G., Marasco, M. & Padovano, M. Ultramafic pseudotachylytes in the Mt. Moncuni peridotite (Lanzo Massif, Western Alps): tectonic evolution and upper mantle seismicity. *Period. Mineral.* **76**, 181–197 (2007).
25. Vitale Brovarone, A. et al. Stacking and metamorphism of continuous segments of subducted lithosphere in a high-pressure wedge: the example of Alpine Corsica (France). *Earth Sci. Rev.* **116**, 35–56 (2013).
26. Debret, B., Nicollet, C., Andreani, M., Schwartz, S. & Godard, M. Three steps of serpentinization in an eclogitized oceanic serpentinization front (Lanzo Massif – Western Alps). *J. Metam. Geol.* **31**, 165–186 (2013).
27. Kienast, J. R. & Pognante, U. Chloritoid-bearing assemblages in eclogitised metagabbros of the Lanzo peridotite body (Western Italian Alps). *Lithos* **21**, 1–11 (1988).
28. Pelletier, L. & Müntener, O. High pressure metamorphism of the Lanzo peridotite and its oceanic cover, and some consequences for the Sesia–Lanzo zone (northwestern Italian Alps). *Lithos* **90**, 111–130 (2006).
29. Rubatto, D., Müntener, O., Barnhoorn, A. & Gregory, C. Dissolution–reprecipitation of zircon at low-temperature, high-pressure conditions (Lanzo Massif, Italy). *Am. Mineral.* **93**, 1519–1529 (2008).
30. Scambelluri, M., Muentener, O., Ottolini, L., Pettke, T. & Vannucci, R. The fate of B, Cl and Li in the subducted oceanic mantle and in the antigorite-breakdown fluids. *Earth Planet. Sci. Lett.* **222**, 217–234 (2004).
31. Lund, M. G. & Austrheim, H. High-pressure metamorphism and deep-crustal seismicity: evidence from contemporaneous formation of pseudotachylytes and eclogite facies coronas. *Tectonophysics* **372**, 59–83 (2003).
32. Lund, M. G., Austrheim, H. & Herambert, M. Earthquakes in the deep continental crust — insights from studies on exhumed high-pressure rocks. *Geophys. J. Int.* **158**, 569–576 (2004).
33. Abers, G. A., Nakajima, J., van Keken, P. E., Kita, S. & Hacker, B. R. Thermal–petrological controls on the location of earthquakes within subducting plates. *Earth Planet. Sci. Lett.* **369–370**, 178–187 (2013).
34. Prieto, G. A., Florez, M. & Barrett, S. A. Seismic evidence for thermal runaway during intermediate-depth earthquake rupture. *Geophys. Res. Lett.* **40**, 6064–6068 (2013).
35. Prieto, G. A., Froment, B., Yu, C., Poli, P. & Abercrombie, R. Earthquake rupture below the brittle–ductile transition in continental lithospheric mantle. *Sci. Adv.* **3**, e1602042 (2017).
36. Andersen, T. B., Mair, K., Austrheim, H., Podladchikov, Y. Y. & Vrijmoed, J. C. Stress release in exhumed intermediate and deep earthquakes determined from ultramafic pseudotachylyte. *Geology* **36**, 995–998 (2008).
37. Dobson, D., Meredith, P. & Boon, S. Simulation of subduction zone seismicity by dehydration of serpentine. *Science* **298**, 1407–1410 (2002).
38. Gasc, J. et al. Simultaneous acoustic emissions monitoring and synchrotron X-ray diffraction at high pressure and temperature: calibration and application to serpentinite dehydration. *Phys. Earth Planet. Int.* **189**, 121–133 (2011).
39. Proctor, B. & Hirth, G. Role of pore fluid pressure on transient strength changes and fabric development during serpentine dehydration at mantle conditions: Implications for subduction-zone seismicity. *Earth Planet. Sci. Lett.* **421**, 1–12 (2015).
40. Ferrand, T. et al. Dehydration-driven stress transfer triggers intermediate-depth earthquakes. *Nat. Commun.* **8**, 15247 (2017).
41. Faccenda, M. & Mancktelow, N. S. Fluid flow during unbending: implications for slab hydration, intermediate-depth earthquakes and deep fluid subduction. *Tectonophysics* **494**, 149–154 (2010).
42. Kita, S., Okada, T., Nakajima, J., Matsuzawa, T. & Hasegawa, A. Existence of a seismic belt in the upper plane of the double seismic zone extending in the along-arc direction at depths of 70–100 km beneath NE Japan. *Geophys. Res. Lett.* **33**, L24310 (2006).
43. Rondenay, S., Abers, G. A. & van Keken, P. E. Seismic imaging of subduction zone metamorphism. *Geology* **36**, 275–278 (2008).
44. Kawakatsu, H. & Watada, S. Seismic evidence for deep-water transportation in the mantle. *Science* **316**, 1468–1471 (2007).
45. Kato, A. et al. Variations of fluid pressure within the subducting oceanic crust and slow earthquakes. *Geophys. Res. Lett.* **37**, L14310 (2010).
46. Angiboust, S., Wolf, S., Burov, E., Agard, P. & Yamato, P. Effect of fluid circulation on subduction interface tectonic processes: insights from thermo-mechanical numerical modelling. *Earth Planet. Sci. Lett.* **357–358**, 238–248 (2012).
47. Ide, S., Shelly, D. R. & Beroza, G. C. The mechanism of deep low frequency earthquakes: further evidence that deep non-volcanic tremor is generated by shear slip on the plate interface. *Geophys. Res. Lett.* **34**, L03308 (2007).
48. Faccenda, M., Burlini, L., Gerya, T. & Mainprice, D. Fault-induced seismic anisotropy by hydration in subducting oceanic plates. *Nature* **455**, 1097–1101 (2008).
49. Angiboust, S. & Agard, P. Initial water budget: the key to detaching large volumes of eclogitized oceanic crust along the subduction channel? *Lithos* **120**, 453–474 (2010).
50. Angiboust, S., Agard, P., Yamato, P. & Raimbourg, H. Eclogite breccias in a subducted ophiolite. A record of intermediate-depth earthquakes? *Geology* **40**, 707–710 (2012).

Acknowledgements

We greatly benefitted from discussions with P. Agard, T. Ferrand, A. Schubnel, O. Onken, E. Cannaò and S. Poli and from constructive comments by T. B. Andersen. We thank M. Kendrick for revising the pre-submission manuscript, and A. Risplendente and L. Negretti for technical assistance during the SEM and wavelength-dispersive spectrometry microprobe work. M.S. and M.G. acknowledge funding by the People Programme (Marie Curie Actions, European Union's Seventh Framework Programme FP7/2007—2013) to the Initial Training Network ZIP (Zooming In-between Plates, REA grant agreement no. 604713). Discussions within ZIP stimulated this work. M.S. also acknowledges support from the Italian MIUR and the University of Genova. G.P. acknowledges funding of the University of Padova.

Author contributions

M.S., G.P. and O.P. wrote the paper. M.S., G.P. and M.G. carried out the fieldwork, and the petrographic and microstructural study. M.B. did the field-emission SEM and EBSD work. O.P. did the TEM work. F.N. did the XRD and Raman analysis. M.S. and G.P. developed the concept.

Competing interests

The authors declare no competing financial interests.

Additional information

Supplementary information is available for this paper at https://doi.org/10.1038/s41561-017-0010-7.

Reprints and permissions information is available at www.nature.com/reprints.

Correspondence and requests for materials should be addressed to M.S.

Publisher's note: Springer Nature remains neutral with regard to jurisdictional claims in published maps and institutional affiliations.

Methods

Moncuni samples were studied by optical and scanning electron microscopes (SEM), an electron microprobe, electron back-scattered diffraction (EBSD) and a transmission electron microscope (TEM). For the SEM analysis, the thin sections were Syton polished and carbon coated (coating thickness of ~3.5 nm).

Optical and scanning electron microscopies were performed at the Universities of Genova in energy-dispersive mode with a SEM VEGA3 TESCAN operating at 15 kV and equipped with an EDAX APOLLO XSDD energy-dispersive X-ray (EDX) spectrometer. Working conditions were 15 kV accelerating potential, 20 nA beam current, 2 µm beam diameter and 100 s counting time.

Major element mineral compositions were analysed by electron probe microanalysis using the JEOL 8200 Superprobe at the Dipartimento di Scienze della Terra, University of Milano. Quantitative elemental analyses were performed by wavelength-dispersive analysis at 15 kV and 60 nA. Natural silicates were used as standards. A PhiRhoZ routine was used for matrix correction. The compositions of feldspar microlites were analysed by EDX spectroscopy at the TESCAN SEM (Erlangen) equipped with the Oxford Instruments INCA system and a 50 mm^2 X-Max detector.

Backscatter secondary electron atomic *Z*-contrast images were collected using a ZEISS CrossBeam 1540 EsB SEM equipped with thermo-ionic field emission at the Department of Material Sciences of the University of Erlangen-Nuremberg.

EBSD analysis was performed using a ZEISS CrossBeam 1540 EsB SEM equipped with the Oxford Instruments Channel5 EBSD system with a Norderly-II camera and Flamenco acquisition software. Working conditions were: (1) 16 mm working distance, 20 kV acceleration voltage, 120 µm aperture and a high current mode resulting in a ~7 nA beam current (with the ZEISS instrument).

Focused-ion beam (FIB) SEM and TEM. Electron-transparent thin foils were prepared for (S)TEM by using a FEI Talos Nanolab G3 UC FIB-SEM. FIB foils were investigated in a FEI Talos F200X (S)TEM equipped with four EDX detectors (Super-X EDX). EDX analyses of submicrometre-sized garnets within the pseudotachylyte were quantified using the Cliff–Lorimer method. All FIB-SEM and TEM analyses were carried out at the Microscopy Square, Utrecht University.

Data availability. All the observations and analytical data supporting the findings of this study are available within the article and its Supplementary Information files. Mineral analyses are reported in the Supplementary Table.